Experimental determination and EHL simulation of transient friction of pneumatic seals in spool valves

Niklas Bauer, Sumbat Bekgulyan, Simon Feldmeth, Frank Bauer, Katharina Schmitz

The transient sealing friction in pneumatic spool valves plays an important role in the dynamics of pneumatic systems. In order to gain a better understanding of this particular tribosystem, an extensive analysis was conducted, combining experimental measurements on a test rig with an elastohydrodynamic lubrication (EHL) simulation model. This contribution presents a description of the test setup and the test conditions, the parametrization of the simulation model and a discussion of the results. Qualitative agreement between theory and measurement has been found. The results indicate that the viscoelasticity of the sealing material as well as the occurrence of starved lubrication conditions cannot be neglected.

1 Introduction

The dynamic behaviour of pneumatic systems depends heavily on the characteristics of its valves. The behaviour of these, in turn, is strongly affected by the tribology of the sealing contacts within the valve. Nowadays, the design of seals for pneumatic valves is based on experimental investigation and experience. However, the exact and complete measurement of the transient friction forces within the sealing contacts is difficult due to the small size and the high dynamics of the system. Since there are many contributing factors which influence the transient friction behaviour of pneumatic seals, many different parameters have to be analysed to accurately describe the dynamics of the seal. In practice, a complete investigation of the behaviour is typically omitted at the expense of the predictability of the valve.

This contribution aims to provide a better understanding of the complex friction behaviour of the sealing contacts in pneumatic spool valves by combining both experimental and simulative investigations. In a first step, a test rig is presented which is capable of measuring the friction force of individual seals and complete set of seals under controlled operating conditions. As a second step, a simulation model is developed which provides a simulation of the elastohydrodynamic lubrication (EHL) within the sealing contacts. For that, an FEM calculation of the deformation of the seal is combined with the solution of the Reynolds equation for obtaining the hydrodynamic pressure within the contact. The model takes into account the non-Newtonian properties of the lubricant, the starved lubrication in the sealing contact as well as the surface topography.

2 Test material

The friction measurements were performed for a pneumatic spool valve. This section describes the used pneumatic valve and its components.

2.1 Pneumatic spool valve

Figure 1 shows a sectional view of a pneumatic spool valve. It consists of a spool within a housing with several ports. In pneumatic systems, these valves are used to control the air flow between components.

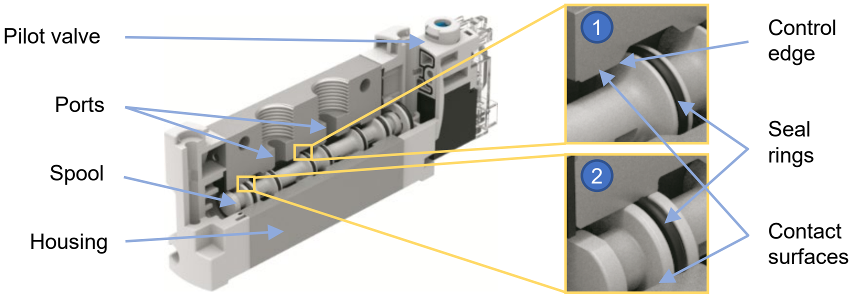

Figure 1: Pneumatic spool valve. Picture provided by courtesy of Festo [1].

During operation, the spool moves within the housing actuated either magnetically with a solenoid or pneumatically by the pilot valve. The position of the spool determines, which ports are connected to or disconnected from each other. In order to prevent internal and external leakage, two different kinds of seals are placed on the spool. The inner seals (1) make or lose contact to the housing depending on the position of the spool and are used in the switching operations to open or close the respective air ports. The two outer seals (2) are always in contact with their counterfaces and seal the pressurized air against the environment. During operation, the relative movement of the seals on their respective counterfaces causes friction. The aim of the presented research is the experimental and simulative determination of the friction within the contact between the housing and the seals.

2.2 Grease

Both, the measurement and the simulation were conducted on a grease with perfluorpolyether base oil (PFPE). The grease is rated NLGI 1 grade. Its temperature range extends from well below $0\ °\mathrm{C}$ to far above $100\ °\mathrm{C}$. The base oil viscosity at $40\ °\mathrm{C}$ is given as about $40\ \mathrm{mm}^2/\mathrm{s}$. The rheological characterisation and EHL simulation of the grease used in the sealing contact of the inner seal are given in [2].

2.3 Seal rings

The friction force measurements were performed for the individual inner and outer seal rings and for the whole valve. The whole valve contains four inner and two outer seal rings on the spool. The inner seal rings are symmetrical in cross-section. During the operation, they make or lose contact to the housing depending on the position of the spool, see Figure 2. Thereby, the inner seal rings are moving over a so-called control edge. Depending on the position on the spool, the inner seal ring closes the gap against (Figure 2, a)) or with (Figure 2, b)) the air pressure.

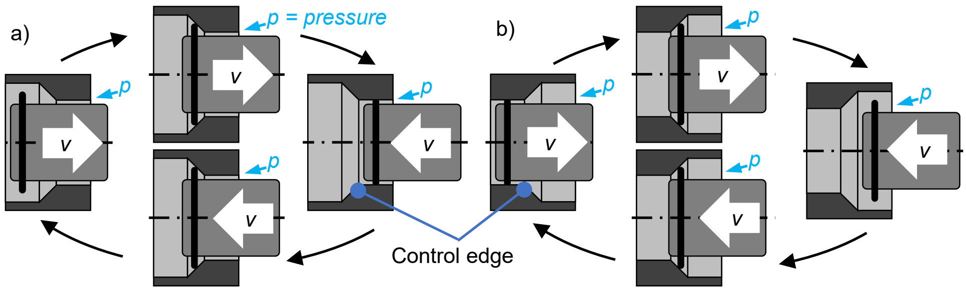

Figure 2: Schematic representation of the spool movement: a) closing the gap against the air pressure, b) closing the gap with the air pressure.

The outer seal rings are not symmetrical in cross-section. They are always in contact with the housing. One of the outer seal rings is on the vented side and is therefore not exposed to pressure. The second outer seal ring have always to seal against the working air pressure from one side.

2.4 Valve housing

During operation, the valve housing acts as the counterface of the seal. Figure 3 shows the six sealing areas of the valve housing. The nominal sealing diameter is $6\ \mathrm{mm}$. The characterisation of the sealing surfaces in the valve housing is given in [3].

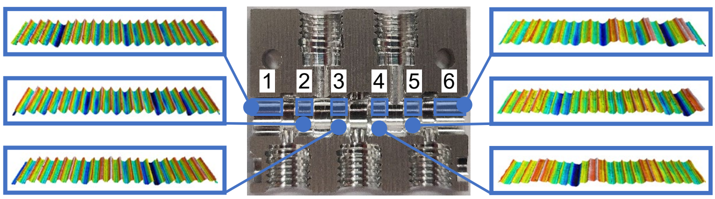

Figure 3: Cross-section of the valve housing with six sealing seats and the representation of optically measured surface topographies [3].

3 Test rig

For the friction force measurements in the sealing contacts of a spool valve, an advanced tribological test method was developed. The test rig is based on a hydropulser MTS 810. Two test set-ups were designed, assembled and put into operation. The first test set-up was designed for the individual investigation of inner and outer seal rings. The second test set-up was designed for the whole valve.

3.1 Hydropulser

The hydropulser MTS 810 is a universal, multipurpose servohydraulic material testing system for static and dynamic translational or axial movement tests. Test parts can be subjected to a displacement or a force load spectrum. The hydropulser consists of the hydraulic power unit and the load unit, see Figure 4.The hydraulic actuator is integrally mounted in the base plate and can translationally move up and down. The force transducer is mounted on the crosshead. The position of the crosshead is locked during the test. An additional force transducer with a $50\ \mathrm{N}$ range was mounted for the friction force measurements.

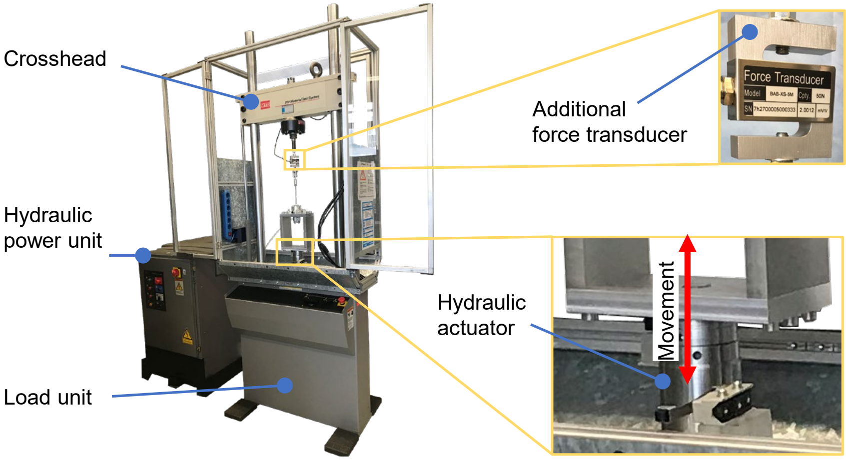

Figure 4: Hydropulser.

3.2 Set-up for an individual seal ring

For the friction force measurement on an individual seal ring, the seal ring is mounted on a rod, see Figure 5. The rod is attached to the stationary force transducer with a double-joint connection. In this way, side forces and moments on the rod can be eliminated. During the test the rod does not move. The valve housing is used as the counterface of the seal. It is connected to a carrier plate, which is joined to the hydraulic actuator and moves during the tests. Also, a bushing housing, which contains an air bushing, is mounted on the carrier plate. The air bushing leads the rod friction free. The centring device on the carrier plate helps to centre the air bushing bore to valve housing bore during the mounting. The space between the air bushing and the test seal ring can be pressurised. The sealing seat diameter and the diameter of the air bushing bore are the same. This means that no axial force is exerted on the rod by the air pressure. Thereby, the force detected by the force transducer is the friction force between the individual seal ring and the valve surface.

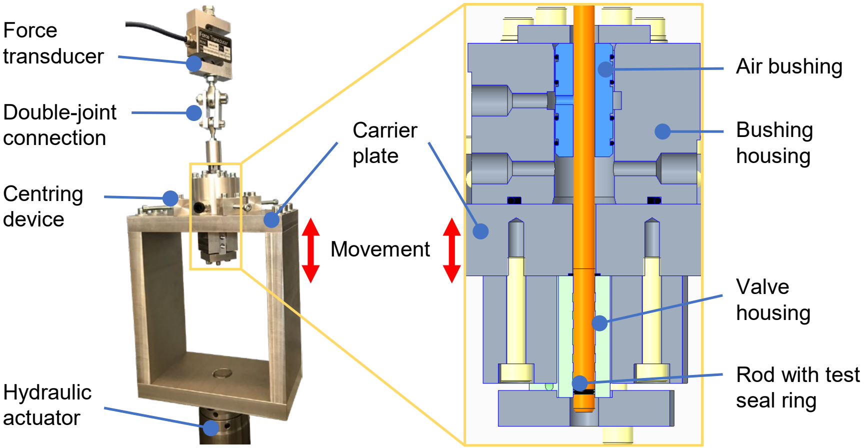

Figure 5: Test set-up for the individual seal ring.

3.3 Set-up for a whole valve

For the friction force measurement on a whole valve, the spool is clamped with a screw in a fastening clamp, see Figure 6. The fastening clamp is attached to the stationary force transducer with the double-joint connection to eliminate side forces and moments on the spool. During the test, the spool does not move. Just like the other set-up, the valve housing is used as the seal counterface. The valve housing is mounted on a housing holder, which is connected to the carrier plate. The carrier plate is fixed to the hydraulic actuator and moves during the tests. Thereby, the friction force between the whole spool with the six seal rings and the valve housing can be measured by the force transducer.

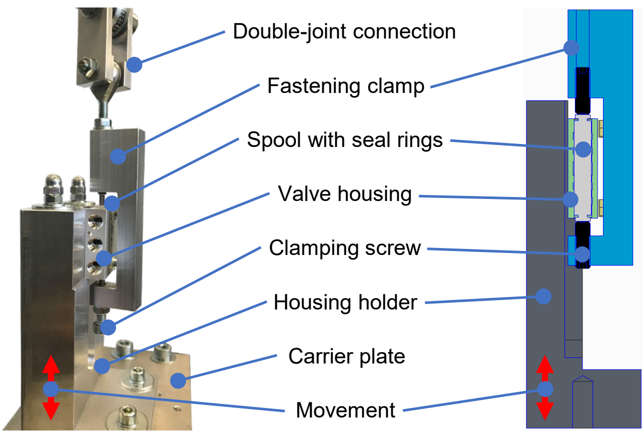

Figure 6: Test set-up for whole valve.

4 Test conditions

To generate the friction, the hydraulic actuator was excited with a cyclic trapezoidal signal, see Figure 7. This signal simulates the movement of the spool in the valve. Within one cycle, the individual seal ring or the spool slides back and forth once. There is a short resting period at each end position. The excitation frequency is $3\ \mathrm{Hz}$. Ten cycles are performed for one measurement. The force and displacement response signals of the 9th cycle are evaluated. The excitation distance is $1.8\ \mathrm{mm}$ for an individual seal ring for testing without moving over the control edge. For testing for an individual seal ring with moving over the control edge and for the whole spool, the excitation distance is $2.7\ \mathrm{mm}$. The nominal excitation speed is $34\ \mathrm{mm/s}$ independent of distance. Measurements with pressure are carried out at $6\ \mathrm{bar}$. All measurements were conducted at room temperature. For all measurements, the seal rings and the sealing seats were lubricated before mounting. Before the measurement, a run-in with 10 000 cycles at the excitation frequency $3\ \mathrm{Hz}$ is performed without air pressure.

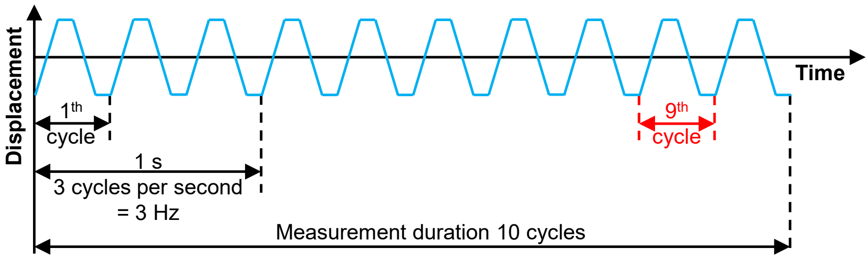

Figure 7: Excitation signal.

5 Simulation model and parameters

For calculating the friction force, the dynamic sealing simulation model ifas-DDS has been used. The ifas-DDS is an EHL simulation tool implemented using the commercial Finite-Element software Abaqus. Originally developed for the calculation of friction and wear of reciprocating hydraulic seals by Angerhausen [4; 5; 6], the ifas-DDS has recently been extended for the description of pneumatic sealing contacts.

5.1 Simulation model

The structure of the ifas-DDS is shown in Figure 8. The simulation model uses a monolithic approach to combine the FEM calculations of the deformation of the seal with the hydrodynamic in the sealing contact as described by the Reynold's equation. The Reynold's equation is extended with Woloszynski's implementation [7] of the Jakobsson-Floberg-Olsson-model [8; 9] to describe cavitation effects and flow factors as introduced by Patir and Cheng [10; 11] to describe the influence of surface roughness.

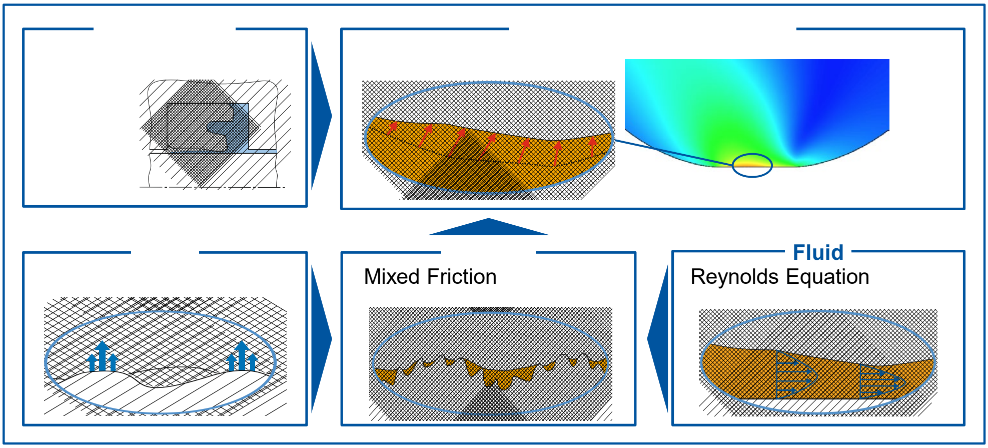

Figure 8: Structure of the dynamic sealing simulation ifas-DDS.

As Figure 8 indicates, the calculated total friction force is obtained by integrating the solid and the fluid shear stress over the contact area. The fluid shear stress τ_{fluid} is calculated based on the shear rate on the seal surface $\dot{\gamma}_{seal}$ and the apparent viscosity of the lubricant at this shear rate $\eta(\dot{\gamma}_{seal})$ according to equation (1):

$$\tau_{fluid} = \eta(\dot{\gamma}_{\mathrm{seal}}) \cdot \dot{\gamma}_{\mathrm{seal}} \tag{1}$$

For the solid shear stress τ_{solid} it is assumed that a constant shear stress τ_c is acting in the real area of contact A_{real}. A_{real} denotes the local percentage of solid contact in the interface of seal and counterface. Thus, the solid shear stress is obtained by multiplying this constant shear stress with the real area of contact:

$$\tau_{solid} = \tau_c \cdot A_{real} \tag{2}$$

With increasing separation, the real area of contact decreases as shown e.g. in [3]. This, in turn, leads to a decrease of solid friction force. Since higher velocities increase the hydrodynamic pressure build-up and thus lead to an increased separation of the contact partners, so that both real area of contact and solid shear stress get reduced. This is the reason why the friction force typically decreases for higher velocities. Currently, there is neither a physical model nor an experimental method to determine the value of τ_c. Therefore, its value has to be determined individually for each sealing system. Currently it is presumed that this parameter is unique for each combination of contacting materials and lubricant.

5.2 Parameters

In contrast to earlier publications [2; 3], the original geometry of the seal has been provided by the partner company and has thus been used for the simulation. Since the geometry is confidential, it is not shown in this paper. All figures displaying the geometry show a simplified geometry which serves as an illustration. This geometry is shown in Figure 9. It has comparable dimensions and similar geometric features. All described effects related to the geometry of the seal have been observed with both geometries. Therefore, the simplified geometry is used for a qualitative discussion of the simulation results. The mesh consists of n_{node} nodes and $n_{elements}$ elements. The mesh is an unstructured quad-dominated mesh using linear axisymmetric hybrid elements of the type CAX3H and CAX4RH.

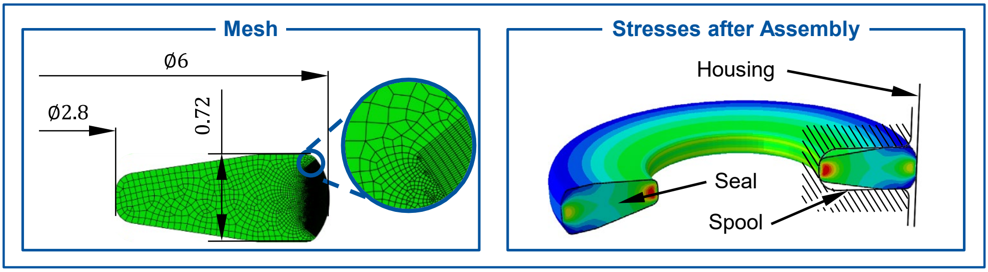

Figure 9: Simplified geometry for illustration purposes.

For the material of the seal, an incompressible hyperelastic Mooney-Rivlin material with the coefficients C_{10} and C_{01} and with the density ρ_{seal} was assumed. The housing and the spool are modelled as rigid bodies. For the contact between seal and spool, a simplified exponential contact behaviour with a constant coefficient of friction $\mu_{Seal-Spool}$ was chosen. The contact between seal and housing is modelled with the EHL simulation. For calculating the normal contact stress and the friction stresses a total of n_{EHL} nodes was used. The parameters of this contact, such as solid contact pressure, real area of contact as well as the pressure and shear flow factor curves have been determined based on the measured surface topography using the commercial software tool TriboX [12]. The results of the determination are presented in [3]. For the grease, non-Newtonian behaviour according to the Palacios-Palacios model [13] with the consistency index k_{PP}, the flow index n_{PP}, the yield stress $\tau_{0,PP}$ and the base oil viscosity $\eta_{b,PP}$ was assumed. The values were calculated according to measurements of the grease at a temperature of $25\ °\mathrm{C}$ as described in [2].

Before the first step of the simulation, spool and housing are positioned with an additional clearance so that there is no contact between seal, housing and spool. In the first step, the model is assembled by removing this additional clearance, which leads to stresses comparable to those shown in Figure 9 (right). In the next step, the seal is moved in a reciprocating pattern, in which the seal is accelerated with constant acceleration a_{const} until the constant velocity v_{max} is reached. After a phase of constant velocity, the velocity is decelerated using the same acceleration followed by the same pattern in opposite direction. This cycle is repeated multiple times. The total distance between both end points is s_{max}.

The values of the parameters used in this paper are shown in Table 1.

Table 1: Parameters of the simulation model.

Parameter	Unit	Value
a_{const}	$\left[\frac{\mathrm{mm}}{\mathrm{s}^2}\right]$	680
C_{10}	[MPa]	0
C_{01}	[MPa]	1.785
k_{PP}	$[\mathrm{Pa\ s}^{n_{PP}}]$	6.7823
n_{EHL}	[−]	226
$n_{elements}$	[−]	3016
n_{nodes}	[−]	3074
n_{PP}	[−]	0.6327
s_{max}	[mm]	1.8
v_{max}	$\left[\frac{\mathrm{mm}}{\mathrm{s}}\right]$	34
$\eta_{b,PP}$	[Pa s]	$94.779 \cdot 10^{-3}$
$\mu_{Seal-Spool}$	[−]	0.15
ρ_{seal}	$\left[\frac{\mathrm{t}}{\mathrm{mm}^3}\right]$	$1.2 \cdot 10^{-9}$
$\tau_{0,PP}$	[Pa]	530.96

6 Experimental results

In the test run, the valve housing was moved and the rod with the seal ring or the spool were fixed. In the real pneumatic valve, the spool moves. The evaluation of the results considers the relative movement between the housing and the spool. Therefore, in the following, the spool or the seal ring is considered movable and the housing fixed. The friction force measurements presented in this work were performed for one individual outer seal ring (sealing seat 1 in Figure 3), two individual inner seal rings (sealing seats 4 and 5 in Figure 3) and the spool with all six seal rings. All specimens were tested with and without the air pressure. The diagrams in the Figure 10 to Figure 13 shows the results as curves of the normalised friction force and the speed over the displacement.

The reference force for normalisation was determined from the friction force without air pressure of the outer seal ring. The outer seal ring always has contact to the counterface in the sealing seat. Thus, there are no severe peaks in the friction force curve. The reference force is the arithmetic mean of the force measured between the positions $-0.5\ \mathrm{mm}$ and $0.5\ \mathrm{mm}$ during the back and forth movement. This corresponds to the force from the middle range of the displacement when sliding at approximately constant speed. Thereby, the influence of starting and braking on the reference force is avoided. In addition, the positions of the seal rings in the sealing seats are schematically shown in Figure 10 to Figure 13.

6.1 Individual outer seal ring

Figure 10 shows the measurement results for the outer seal ring. The friction force that occurs when sliding with pressure is more than twice as high as when sliding without pressure. Once the sliding starts, the force increases rapidly. As the sliding continues, the force decreases slightly. The force decrease is higher when sliding with pressure than without pressure.

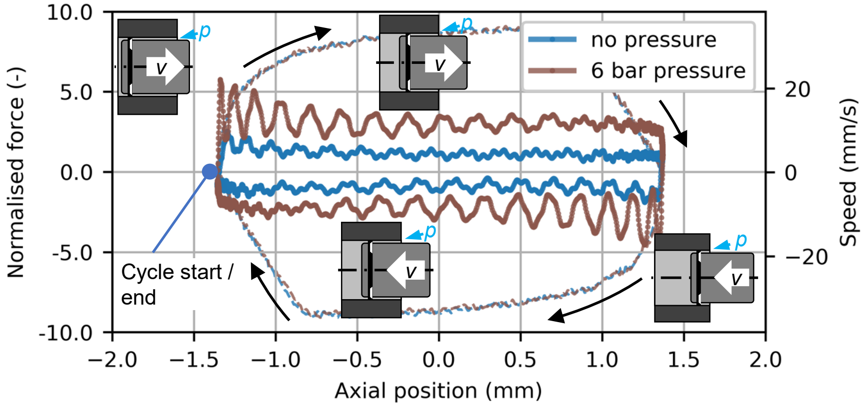

Figure 10: Outer seal ring.

6.2 Individual inner seal ring (gap closing against air pressure)

Figure 11 shows the results for the inner seal ring, sliding at sealing seat 5 (nomenclature according to Figure 3). At this position, the seal ring closes the gap against the air pressure when it hits the control edge. The seal ring starts in the air without contact to the sealing seat. The hit on the control edge causes a peak in the force curve. After that, the seal ring slides on the counterface. During backward sliding, the seal ring opens the gap when leaving the sealing seat at the control edge. The friction force amount decreases. The friction force that occurs when sliding with pressure is higher than when sliding without pressure. The force peak without pressure is about twice as high as the following friction force. The force peak with pressure is about five times as high as the following friction force and the peak without the pressure. The force peak with pressure is slightly offset from the peak without the pressure. There are oscillations in the measured friction force, the cause of which was intensively and systematically investigated parallel to the friction force measurements. The oscillations are caused by the oscillation behaviour of the mechanical measuring chain. In the test set-up for an individual seal ring, the mechanical measuring chain consists of the force transducer, double-joint connection and rod. The natural frequency of this measuring chain is approx. 157 Hz. This frequency, which is independent of the excitation speed, corresponds exactly to the oscillations in the friction force curve of the individual seal ring. The amplitude of the oscillations varies with the test conditions and cannot be specified clearly until now.

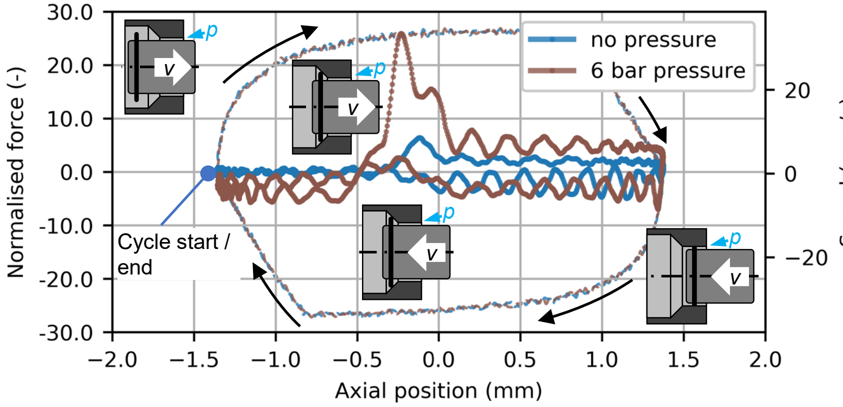

Figure 11: Inner seal ring, gap closing against air pressure.

6.3 Individual inner seal ring (gap closing with air pressure)

Figure 12 shows the results for the inner seal ring, sliding on sealing seat 4 (Figure 3). At this position, the seal ring closes the gap with the air pressure when it hits the control edge. The seal ring starts to slide in the sealing seat. When leaving the sealing seat at the control edge, the seal ring opens the gap and the friction force amount decreases.

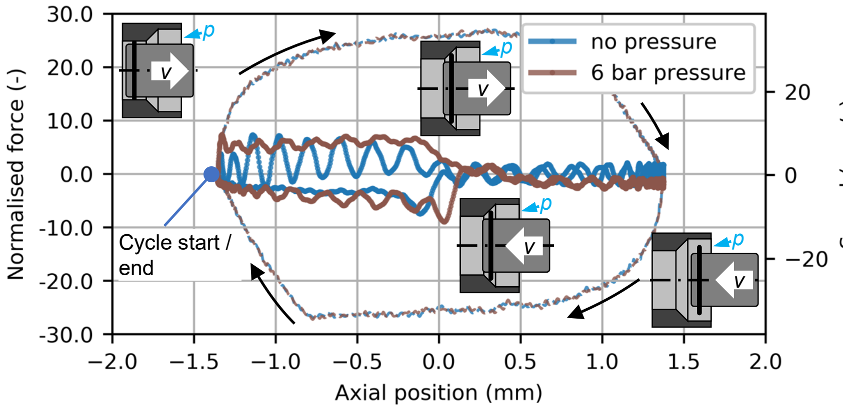

Figure 12: Inner seal ring, gap closing with air pressure.

During backward sliding, the seal ring hits the control edge. That causes a peak in the force curve. After that, the seal ring slides on the counterface. The friction force that occurs when sliding with pressure is higher than when sliding without pressure. The force peak without pressure is more than twice as high as the following friction force. The force peak with pressure is about half higher than the following friction force. The force peak with pressure is only 15 % higher than without pressure. The force peak with pressure is slightly offset from the peak without the pressure.

6.4 Whole valve

Figure 13 shows the results for the whole spool with all six seal rings. During operation, only four of six seal rings are in contact with the sealing seats at the same time. Both outer seal rings are always in contact. The inner seal rings are only in contact in pairs. Either the seal rings in sealing seats 2 and 4 or 3 and 5 (Figure 3) are in contact with the counterface. In this way, one seal rings pair hits the control edge at approximately the same time as the other seal rings pair leaves the sealing seats. The friction forces of the individual seal rings on the spool overlap. Thus, the friction force in the whole valve is higher than the friction of each individual seal ring. The friction force with pressure is higher than without pressure. The force amounts before and after the peaks are approximately at the same level. When sliding in positive direction, the force peak is three times higher than the force after the peak. When sliding back, the peak is only two times higher as the force after the peak. This qualitatively corresponds to the curves of the individual seal rings in Figure 11 and Figure 12. The friction force shows a slight decrease shortly before the peak. This can be caused by a slight time offset between the moments when the seal rings hit or leave their control edges.

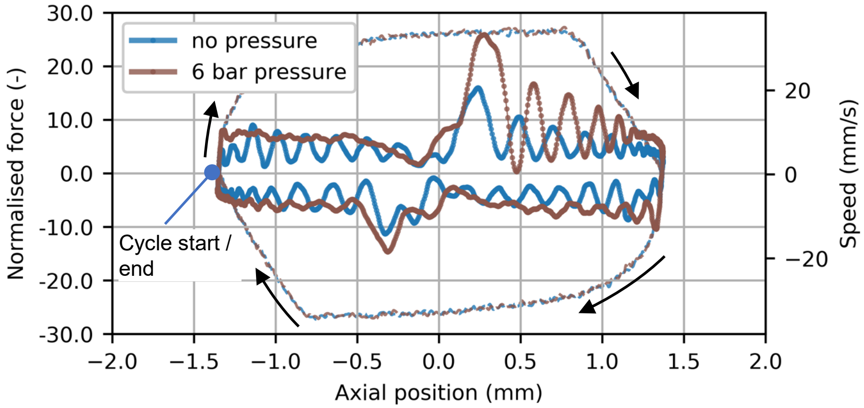

Figure 13: Whole valve.

7 Simulation results

This chapter starts by discussing the shares of solid and fluid friction for an inner seal ring without pressure in section 7.1. In addition, the reason for the visible hysteresis is discussed. Section 7.2 provides an investigation of the influence of the solid shear stress τ_c. Finally, a comparison and discussion of simulated and measured friction force is presented in sections 7.3 and 7.4.

The presented simulation results were normalised in the same manner as the experimental results and use the same experimentally determined value for normalisation as described in chapter 6. Note, that this contribution shows simulation results for the inner ring without pressure difference. The friction force of the outer ring and the influence of the pressure force are currently investigated and will be presented in another publication.

7.1 Explanation of the hysteresis

Figure 14 shows the calculated friction force for an inner seal ring without pressure and without moving over a control edge. Here, a distance of $3\ \mathrm{mm}$ between the end points and a solid shear stress $\tau_c = 1.5\ \mathrm{MPa}$ was assumed. It can be seen that the largest share of the total friction force is the solid friction force with a share of more than $90\ \%$. Additionally, it can be seen that the solid and fluid friction force show an opposite tendency regarding the velocity. The fluid friction increases with increasing velocity due to higher shear rates in the contact. The solid friction force, however, decreases for higher velocities due to the smaller separation caused by lower hydrodynamic pressure in the contact.

As for the total friction force, a similar tendency as for the solid friction force can be observed. During acceleration, the total friction force decreases. Immediately after the constant velocity is reached, the total friction force still continues to drop for a short time after which a steady state with constant friction force is reached. During deceleration, the friction force increases again due to the smaller separation of surfaces and thus smaller hydrodynamic pressure build-up.

Close to the end points, a hysteresis can be observed, during which the friction force acts in the same direction as the relative velocity thus supporting the movement, e.g. at points (1) and (4)). An explanation of this hysteresis is given in Figure 14 (bottom). When the movement starts, the seal is still prestressed by the tangential stresses of the movement in the opposite direction (1). When the movement starts, these prestresses are continuously reduced by the movement of the counterface until the seal reaches its unstressed position of rest in the static equilibrium. As the movement continues, elastic deformation of the seal occurs again, leading to a force counteracting the movement of the counterface (2). At a position of about $-1.4\ \mathrm{mm}$, the friction force starts to decrease again. The reason for this decrease is the axial clearance between seal and spool. This leads to two stable equilibria and one unstable equilibrium of the system. The stable equilibria are reached when the seal bends either to the left or to the right end point. Between these, there is the unstable equilibrium during which no friction occurs (3). When the spool continues to move beyond the unstable equilibrium, the seal tries to move towards the next stable equilibrium, which is the right end point. This again causes a force acting in the same direction as the movement (4). After the end point is reached, the friction force rises almost linearly due to elastic deformation of the seal (5). When the elastic deformation reaches its maximum, the seal starts to slide on the counterface. The friction force decreases with increasing velocity due to the hydrodynamic pressure (6).

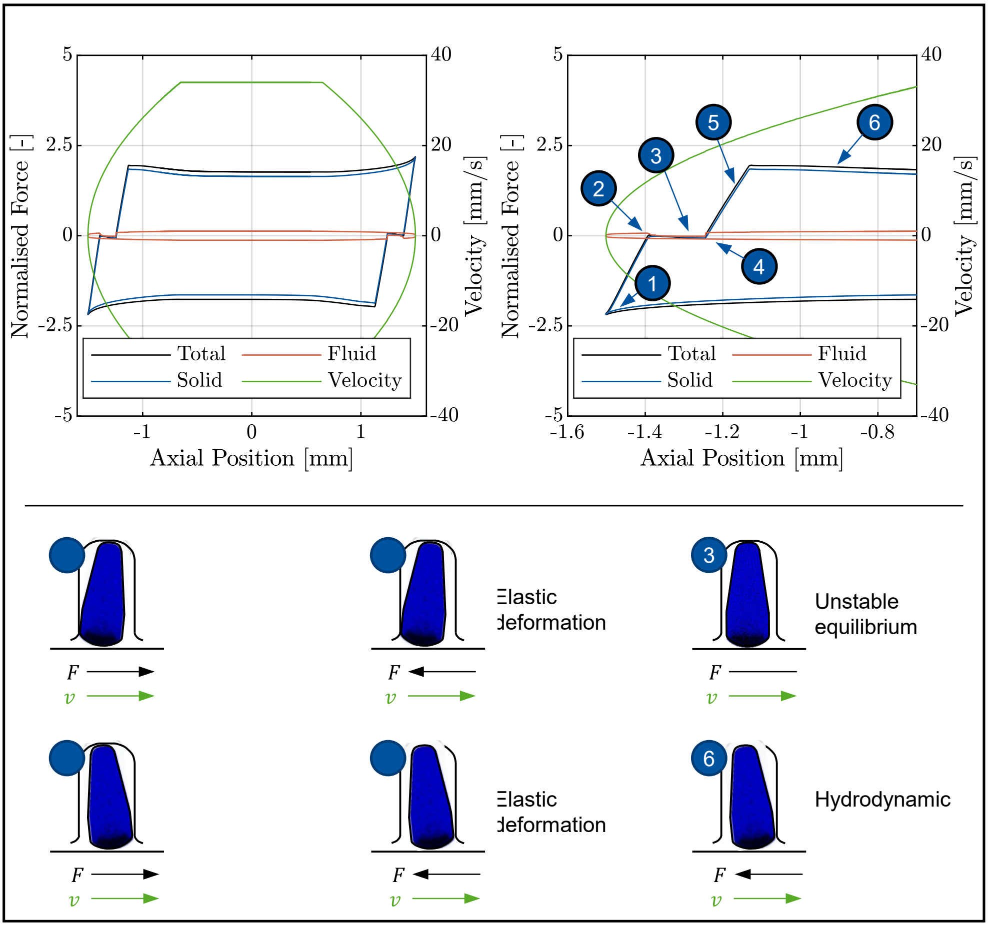

Figure 14: Top left: Simulation results of the friction force without control edge. Top right: Detail view. Bottom: Illustration of the bistability causing the hysteresis.

7.2 Influence of the solid shear stress τ_c

Since the solid shear stress τ_c is a parameter that currently cannot be determined experimentally, a parameter study was conducted. For this purpose, the simulation presented in the previous chapter has been repeated with different values of the solid shear stress τ_c. In total, nine simulations were conducted, with the values of τ_c ranging from $0.5\ \mathrm{MPa}$ up to $2.5\ \mathrm{MPa}$ increased with an increment of $0.25\ \mathrm{MPa}$ after each simulation. The calculated total friction forces are shown in Figure 15 (left). As expected, higher values of τ_c lead to higher friction forces. In addition, it can be seen, that the general shape of the curves remains the same. Since the shape of the curves remains the same, it is suspected that the hydrodynamic conditions in the contact are largely unaffected by the value of τ_c. Thus, assuming a constant real area of contact, the solid friction force is proportional to the solid shear stress τ_c according to equation (2). Given that the largest share of the total friction force is contributed by the solid force, it seems likely, that the total friction force is also roughly proportional to the solid shear stress τ_c. If this conjecture is correct, the quotient of total friction force and solid shear stress should be the same for all nine simulations. This quotient is depicted in Figure 15 (right).

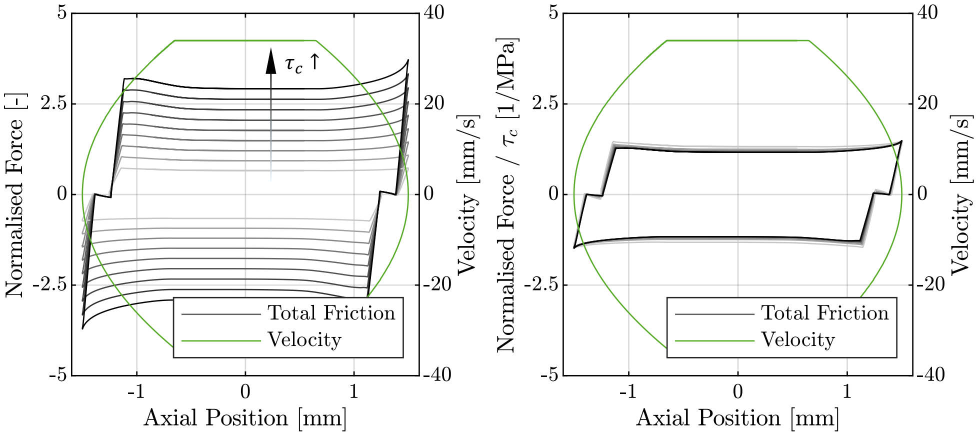

Figure 15: Left: Influence of the solid shear stress τ_c on the total friction force. Right: Total friction force divided by the solid shear stress τ_c

It can be seen that all curves are nearly laying upon each other. Therefore, it is concluded that the total friction force is indeed proportional for the investigated range of $\tau_c = 0.5 \ldots 2.5$ MPa, within an error tolerance of about 15 %. The largest deviations occur for small values of τ_c. This is because with lower solid shear stresses, the share of fluid friction becomes higher. However, the assumption that the total friction force is proportional to the solid shear stress neglects the fluid friction. This leads to an underestimation of the friction forces for smaller values of τ_c as depicted in Figure 15 (right).

7.3 Comparison of simulation and measurement

A comparison of simulation and measurement for an inner seal ring is presented in Figure 16. For the simulation, a value of $\tau_c = 1.5$ MPa was chosen arbitrarily. In order to make a comparison of simulation and experiment easier, the measurement was filtered by a moving average filter with a step width of 50. Since the simulation model does not contain the whole measuring chain, their natural resonance is not simulated. Thus, the oscillations caused by natural resonance in the measurements are ignored during the comparison.

Figure 16 (left) shows a comparison for the setup during which the seal does not move over the control edge. The setup which moves over the control edge is shown in Figure 16 (right). For both setups, similarities and differences can be observed. As for the similarities, the same almost constant friction force during the movement with constant velocity is observed for both setups (1). Similarly, the shape of the rising friction force when the seal ring makes contact with the housing (2) as well as the decrease while losing contact (3) match the tendency in the measurement. However, the decrease in friction force during deceleration which is visible in the measurements does not occur in the simulation (4). Instead, the calculated friction force increases during deceleration. Another deviation occurs right after that, when the velocity increases again. The previously discussed hysteresis is not visible in the measurements (5). Finally, the magnitude of the simulation results does not match the measurements. While the total friction force is too high for the case without moving over the control edge, the calculated forces are too low for the movement over the control edge. This is especially visible for the peak after making contact (6).

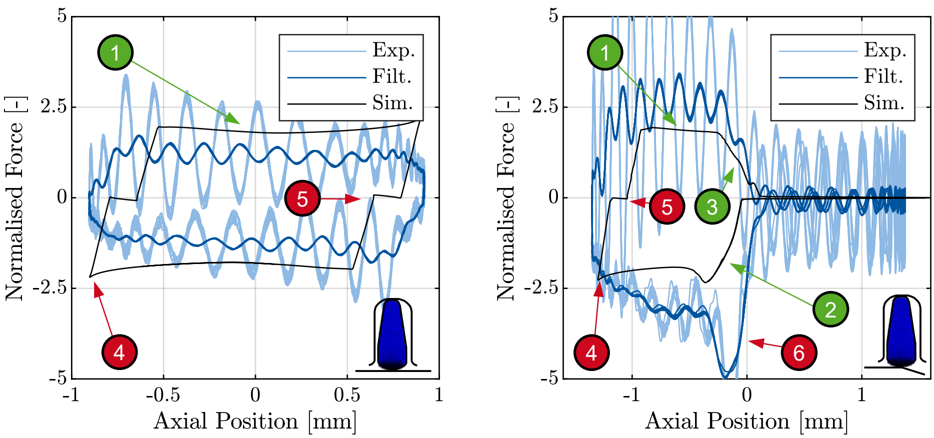

Figure 16: Comparison of measured (filtered and unfiltered) and simulated friction force. Left: Without moving over the control edge. Right: With moving over the control edge.

7.4 Discussion of the deviations

The observed increase in calculated friction force during deceleration is in line with the expectations of the lubrication theory. As the velocity decreases, the hydrodynamic pressure is lower, which leads to smaller separations and higher friction forces. The fact that it cannot be observed in the experiment might indicate that starved lubrication occurs during the motion. This condition describes that the available lubricant is not sufficient to separate the contacting surfaces as far as the Reynolds equation predicts. It is expected, that once starved conditions are reached, a further increase in velocity does not reduce the friction force, since there is not enough lubricant to further separate the contacting surfaces. Instead, the friction force might even decrease with decreasing velocity if the deceleration occurs on a part of the counterface with more lubricant available. This could be an explanation of the behaviour observed in Figure 16 (4). In order to improve the simulation, the film generation of the seal needs to be considered, e.g. as described by Feuchtmüller et al. [14].

The absence of the hysteresis depicted in Figure 14 in the measured data indicates that the seal cannot move as far in axial direction as in the simulation model. A possible explanation for this is that the groove between seal and spool is filled by grease preventing axial movement of the seal. This can be accounted for in the simulation model by applying an appropriate boundary condition. However, it should be noted that due to the oscillations in the measured forces, hysteresis might occur in the experiment. Therefore, it might be possible that there is a hysteresis which is not visible in the plotted friction force, even though it is expected that the axial movement is indeed hampered by grease inside the groove. Anyway, it is expected that the described axial movement will not occur in the simulation once air pressure is applied since the seal will be pressed against one side of the groove by the pressure difference.

Finally, the difference in magnitude between measurement and calculation might occur due to the viscoelasticity of the seal material. Generally, the absolute value of the simulation results can be easily scaled by selecting the parameter τ_c as presented in chapter 7.2. However, it was expected that one single value of τ_c is sufficient to describe both cases with and without moving over the control edge. As shown in Figure 16, for the case without moving over the edge, a value smaller than $\tau_c = 1.5\ \mathrm{MPa}$ should be selected, whereas for the simulation with moving over the control edge, a larger value appears to be necessary. This is where the viscoelasticity comes into play. It can be seen that the friction forces at positions left of $-0.5\ \mathrm{mm}$ are about twice as high for the measurements where the seal moved over the control edge before. In contrast to that, the calculated forces have roughly the same magnitude regardless of whether the seal passed the control edge earlier or not. Assuming similar surface properties and lubrication condition, this indicates, that passing the control edge somehow increases the friction force even after both surfaces are in complete contact. Rubber materials typically show viscoelastic behaviour, meaning their stiffness increases with higher load frequency. For the inner seal ring the counterface acts as a constant normal load when it does not pass over the control edge, i.e. the normal force has a load frequency of zero. However, during the experiment where the seal ring moves over the control edge, the normal load is oscillating between zero and the maximum with a frequency equal to the frequency of the excitation signal. This would therefore cause the seal material to act stiffer, in turn leading to higher normal and thus also tangential stresses in the sealing contact.

8 Summary and conclusion

An extensive analysis of the sealing friction of a pneumatic spool valve has been presented. The friction force of individual seals as well as the complete valve has been measured. In addition, a simulation model was used to calculate the friction force for one kind of seal ring.

For the friction force measurements, an advanced tribological test method was developed. Two test set-ups were designed, assembled and put into operation. The first test set-up was designed for measurements on an individual seal ring with and without pressure. The second test set-up was for the whole valve. The experimental results show jumps in the friction force curves when sliding over the control edge. The friction force that occurs when sliding with pressure is higher than when sliding without pressure.

The simulation results show, that the friction force in the observed operating conditions are dominated by solid friction. Accordingly, the parameter τ_c which denotes the solid shear stress acting on the real area of contact is almost proportional to the total friction force. As for the comparison between simulation and experiment, a qualitative agreement between both methods was found. While the general shape of the measured data can be predicted quite well using the simulation model, there are deviations regarding certain features and the overall magnitude. Possible explanations have been discussed and will be further investigated in the future. Especially the impact of the viscoelasticity of the material and starved lubrication conditions are expected to have a considerable impact on both magnitude and qualitative behaviour of the calculated friction force. Additionally, the calculations presented in this paper use a simplified kinematic. It is planned to run the simulations using the real kinematic of the experiment by directly importing the measured position data from the test rig. For further comparisons between simulation and experiment, the simulation approach will also be used to calculate the friction force between the outer seal rings and the counterface as well as the influence of the air pressure.

9 Acknowledgements

The authors thank the Research Association for Fluid Power of the German Engineering Federation VDMA for its financial support. Special gratitude is expressed to the participating companies and their representatives in the accompanying industrial committee for their advisory and technical support.

10 Nomenclature

Variable	***Description***	***Unit***
a_{const}	Constant acceleration during simulation	$\left[\frac{\mathrm{mm}}{\mathrm{s}^2}\right]$
A_{real}	Percentage of real area of contact	$[-]$
C_{10}	Mooney-Rivlin parameter	$[\mathrm{MPa}]$
C_{01}	Mooney-Rivlin parameter	$[\mathrm{MPa}]$
k_{PP}	Consistency index of the used grease	$[\mathrm{Pa\ s^n}]$

n_{EHL}	Number of nodes used for calculating the EHL contact	$[-]$
$n_{elements}$	Total number of Elements in the FEM model	$[-]$
n_{nodes}	Total number of nodes in the FEM model	$[-]$
n_{PP}	Flow index of the grease	$[-]$
s_{max}	Excitation distance in the simulation	$[\mathrm{mm}]$
v_{max}	Maximum velocity in the simulation	$\left[\frac{\mathrm{mm}}{\mathrm{s}}\right]$
$\dot{\gamma}_{seal}$	Shear rate on the seal surface	$\left[\frac{1}{s}\right]$
η	Apparent viscosity	$[\mathrm{Pa\ s}]$
$\eta_{b,PP}$	Base oil viscosity of the grease	$[\mathrm{Pa\ s}]$
$\mu_{Seal-Spool}$	Constant coefficient of friction between seal and spool	$[-]$
ρ_{seal}	Density of the seal	$\left[\frac{\mathrm{t}}{\mathrm{mm}^3}\right]$
$\tau_{0,PP}$	Yield stress of the grease	$[\mathrm{Pa}]$
τ_c	Constant shear stress acting on real area of contact	$[\mathrm{Pa}]$
τ_{fluid}	Fluid shear stress	$[\mathrm{Pa}]$
τ_{solid}	Solid shear stress	$[\mathrm{Pa}]$

11 References

[1] Festo SE & Co. KG. 2018. *Info Valve and valve terminal series VG* [online]. Available at https://www.festo.com/net/SupportPortal/Files/381028/PSIplus_VTUG_en_V05_M.pdf last visited 12. August 2021].

[2] Bauer, N. et al. 2021. *Rheological Characterization and EHL Simulation of a Grease in a Lubricated Sealing Contact* [online]. Tribologie und Schmierungstechnik. doi: 10.24053/TuS-2021-0034.

[3] Bauer, N. et al. 2022. *EHL Simulation of Transient Friction of Translational Seals in Pneumatic Spool Valves under Consideration of 3D Surface Topography Measurement Data.* 13th International Fluid Power Conference Aachen (IFK 2022).

[4] Angerhausen, J. et al. 2018. *Influence of transient effects on the behaviour of translational hydraulic seals* [online]. Fluid power networks : proceedings : 19th - 21th March 2018 : 11th International Fluid Power Conference. doi: 10.18154/RWTH-2018-224540.

[5] Angerhausen, J. et al. 2019. *Simulation and experimental validation of translational hydraulic seal wear* [online]. Tribology International. doi: 10.1016/j.triboint.2019.01.048.

[6] Angerhausen, J. 2020. *Physikalisch motivierte, transiente Modellierung translatorischer Hydraulikdichtungen*. Dissertation. Aachen.

[7] Woloszynski, T. et al. 2015. *Efficient Solution to the Cavitation Problem in Hydrodynamic Lubrication* [online]. Tribology Letters. doi: 10.1007/s11249-015-0487-4.

[8] Jakobsson, B. und Floberg, L. 1957. *The finite journal bearing, considering vaporization*. Transactions of Chalmers University of Technology. 190.

[9] Olsson, K.-O. 1965. *Cavitation in dynamically loaded bearings*. Transactions of Chalmers University of Technology. 308: 59.

[10] Patir, N. und Cheng, H. 1978. *An Average Flow Model for Determining Effects of Three-Dimensional Roughness on Partial Hydrodynamic Lubrication* [online]. Journal of Lubrication Technology. doi: 10.1115/1.3453103.

[11] Patir, N. und Cheng, H. 1979. *Application of Average Flow Model to Lubrication Between Rough Sliding Surfaces* [online]. Journal of Lubrication Technology. doi: 10.1115/1.3453329.

[12] Tribo Technologies. 2021. *Tribo-X* [online]. Available at https://www.tribo-technologies.com/de/tribo-x last visited 20. September 2021].

[13] Palacios, J. und Palacios, M. 1984. *Rheological properties of greases in ehd contacts* [online]. Tribology International. doi: 10.1016/0301-679X(84)90010-0.

[14] Feuchtmüller, O. et al. 2021. *Remarks on Modeling the Oil Film Generation of Rod Seals* [online]. Lubricants. doi: 10.3390/lubricants9090095.

12 Authors

RWTH Aachen University, Institute for Fluid Power Drives and Systems (ifas)

Campus-Boulevard 30, 52074 Aachen, Germany:

Niklas Bauer, M. Sc., ORCID 0000-0002-5520-0611, niklas.bauer@ifas.rwth-aachen.de

Univ.-Prof. Dr.-Ing. Katharina Schmitz, ORCID 0000-0002-1454-8267, katharina.schmitz@ifas.rwth-aachen.de

University of Stuttgart, Institute of Machine Components (IMA)

Pfaffenwaldring 9, 70569 Stuttgart, Germany:

Dipl.-Ing. Sumbat Bekgulyan, ORCID 0000-0003-0446-2264, sumbat.bekgulyan@ima.uni-stuttgart.de

Dipl.-Ing. Simon Feldmeth, ORCID 0000-0003-0018-0710, simon.feldmeth@ima.uni-stuttgart.de

PD Dr.-Ing. Frank Bauer, ORCID 0000-0001-7799-7628, frank.bauer@ima.uni-stuttgart.de